ISSN (Online): 2455-3662
EPRA International Journal of Multidisciplinary Research (IJMR) - Peer Reviewed Journal
Volume: 12| Issue: 6| June 2026|| Journal DOI: 10.36713/epra2013 || SJIF Impact Factor 2026: 8.753 || ISI Value: 1.188

THERMO-KINETICS ANALYSIS OF DATE PALM FRONDS DURING PYROLYSIS AND GASIFICATION USING TGA TECHNIQUES

Mutaz Hassan[a], Bakheit Mustafa Bakheit[a], Ibrahim Khalil Adam[a*], Elbager M.A.Edreis [a], Swellam W. Sharshir [b] Hong Yao[c]

[a] *Mechanical Engineering Department, Blue Nile University, 143, Er Roseires, Ad Damazin, Sudan.*
[b] *Mechanical Engineering Department, Faculty of Engineering, Kafrelsheikh University, Egypt.*
[c] *State Key Laboratory of Coal Combustion, School of Energy and Power Engineering, Huazhong University of Science and Technology, Wuhan, Hubei 430074, People`s Republic of China.*

ABSTRACT

In this study, the effects of pyrolysis and gasification temperatures (800, 900 and 1000 ˚C) on the reactivity, behaviours, kinetic and thermodynamics parameters of date palm fronds (DPF) were investigated using a thermogravimetric analyzer (TGA). Homogeneous model (HM) or the first-order chemical reaction (O1) and shrinking core models (SCM) or Phase boundary-controlled reactions (R2 and R3) were used to estimate the kinetics and thermodynamics parameters. The temperature is found to have significant effects on gasification compared to the pyrolysis process. The gasification process showed two stages of combustion at 900 and 1000 °C, but for the pyrolysis, it was one at 800 °C. The mean reactivity was directly proportional to pyrolysis temperature. However, for the gasification, the mean reactivity increased as the temperature increased up to 900 °C, before it decreased as the temperature reached 1000 °C. The gasification process at 900 °C showed lower values of activation energy, pre-exponential factor and reaction rate compared to those at 800 and 1000 °C. Average enthalpy change was 3.85 and 7.10 % higher in stage 1 with the O1 and R3 model, respectively, compared to the R2 model. The average Gibbs free energy for the R3 model was 0.3– 2.7% higher in stage 1 than the R2 and O1 model. However, the change of entropy for the samples investigated was found to be insignificant. Finally, all the models are successfully utilized to predict the experimental data under both processes at the investigated temperature.

KEYWORDS: *Date Palm Frond, Pyrolysis, Gasification, Kinetics, Thermodynamic Parameters.*

1. INTRODUCTION

Biomass utilization for energy usage has increased because of its economic and environmental benefits [1]. Biomass is an organic material such as sugar cane, straw, wood waste, date palm fronds, and different varieties of agricultural and industrial waste products [2]. Gasification is an efficient and advanced technology for extracting energy from biomass [3]. It is divided into two stages after the initial short drying: devolatilization (pyrolysis) and char gasification. The char gasification process is a much slower conversion process compared to the initial pyrolysis, thus it is dominant in the whole gasification process [4, 5]. Date palm fronds are the branching parts of date palm trees. According to the Food and Agriculture Organization, 1.14 million hectares were cultivated, and the tree sheds 14─20 kg annually. This could achieve up to 3.4 million tons of date palm fronds annually, depending on tree density per hectare.

Sudan ranks in 8th place worldwide in date production. However, due to the lack of technologies, the fronds waste is burned traditionally for cooking and other uses [6]. However, few studies were focused on the date palm fronds thermal conversion process. Jeguirim et al. [7] examined the behavior of date palm leaflets, date palm rachis, date palm trunk, date stones, and fruitstalk prunings using a thermogravimetric analyzer under non-isothermal conditions. Ultimate and proximate analyses showed that date stones have high energy density among the samples. The thermal degradation of the samples was found to be similar, except for the date stones. Date palm trunk was the most reactive at both oxidative atmosphere and pyrolysis, whereas a date stone was less reactive. The activation energies for the tested samples were in the range of 45.2– 89.1 and 49.6– 110.7 kJ mol^{-1} for pyrolysis and oxidation. Cardoso et al. [8] studied thermal decomposition of sorghum bagasse and tobacco waste at non-isothermal thermogravimetric conditions. The activation energy was 103.94 and 120.01 kJ/mol for tobacco waste and sorghum bagasse, respectively using Ozawa method, respectively. However, for the Starink method, these values were -135.95 and 148.91 kJ/mol for tobacco waste and sorghum bagasse, respectively. For the independent parallel reaction model, activation energy values were in the range of 39.7–272.0 and 35.7–220.0 kJ/mol for tobacco waste and sorghum bagasse , respectively. Okoroigwe et al. [9] studied the devolatilization characteristics and kinetics of Gmelina, Mango, Neem, and Tropical Almond woods under synthetic air conditions at a heating rate of 30 °C/min. Non-isothermal thermogravimetric analysis at temperature of 30 and 750 °C under synthetic air was used. The samples were found to follow two stages reactions at a

ISSN (Online): 2455-3662
EPRA International Journal of Multidisciplinary Research (IJMR) - Peer Reviewed Journal
Volume: 12| Issue: 6| June 2026|| Journal DOI: 10.36713/epra2013 || SJIF Impact Factor 2026: 8.753 || ISI Value: 1.188

temperature range of 200– 500 ºC, which indicated volatile oxidation and char combustion. The weight losses were 2.20, 1.50, 1.25 and 1.60 for Gmelina, Mango, Neem and Tropical almond woods, respectively, and occurred at peak temperatures of 310, 322, 320 and 320 ºC. At the oxidative stage, the activation energies with the Arrhenius model are 125,108, 142 and 113 kJ/mol, respectively, for Gmelina, Mango, Neem and Tropical almond woods, while at the char combustion stage, these values were 257, 210, 281 and 345 kJ/mol, respectively. Raza et al. [10] studied the thermo-kinetics and thermodynamic analyses of date palm surface fibers (DPSFs) using thermogravimetric analysis. DPSFs were heated non-isothermally from 20 to 800 ˚C at a temperature rate of 10 ˚C/min in a nitrogen atmosphere. Thermogravimetric analysis showed two stages for pyrolysis. The low-temperature stable components were decomposed in a temperature range of 270─390 ˚C and the high-temperature stable components were degraded in a temperature range of 390─600 ˚C. Ginstlinge Brounshtein and Ginstling diffusion models were the best fitted models with the highest regression coefficient values (R2 > 0.99) in both mass-loss regions. The activation energy values were found to be 96─ 98 and 113─ 114 kJ/mol, respectively. El-Sayed et al. [11] investigated thermal degradation of palm fronds (PF), olive leaves (OL), and wheat straw (WS) through pyrolysis and calculated kinetic data using TG-DTG and DTA. Ozawa-Flynn-Wall (OFW) and Kissinger–Akahira–Sunose (KAS) methods, as well as model-fitting techniques like the integral method, were used for kinetics studies. For PF, OL, and WS, the activation energy from the integral method ranged between 8.82 ─167.13, 23.06 ─ 149.20, and 11.01─ 156.27, respectively. For the reaction order model, the activation energies were 22.3 ─ 117.49, 51.69 ─ 92.88, and 23.48 ─ 125.97, respectively. Ali et al.[12] studied the process optimization and economic evaluation of air gasification of date palm fronds (DPF. The temperature was the most influential factor for H_2 composition, compared to air flow rate and feedstock particle size. The optimum conditions were 900 ℃, 1 l/min air flow rate, and 6 mm feed stock particle size. Galiwango et al.[13] investigated date palm wastes (leaflet, rachis, fibers, and their composite) at non-isothermal combustion kinetics using the thermogravimetric technique. Thermogravimetric analysis results showed a major peak for the degradation of volatiles between 127–138 ºC with average percentage mass loss of 68.04 ± 1.5, 65.57± 0.6, 62.97 ± 5.5, and 59.26 ± 3.2, for rachis, composite, leaflet, and fibers, respectively. The positive enthalpy values confirmed an endothermic pyrolysis reaction. A minimal defference of 4.40─ 7.51 kJ mol^{-1} between activation energy and enthalpy for rachis, fibers, composite, and leaflet ensued, respectively. Wang et al. [14] studied co-gasification properties of petroleum coke and millet husk biomass char and their blends using thermogravimetric analysis under steam atmosphere conditions. The activation energy was calculated using random pore, volumetric and unreacted-core models. Random pore model was better describing char co-gasification compared to volumetric and unreacted-core models. Xu et al. [15] studied the kinetic behavior of CO_2 gasification for three types of coal (lignite, bituminous coal and lean coal) and biomass (Sawdust, Rice straw, and Corn stalk) samples using a thermogravimetric analyzer. The activation energy was estimated using the homogeneous reaction model and the shrinking core model. The activation energy decreases as the sawdust content increases. Edreis , et al. [16] investigated, the H_2O co-gasification of petroleum coke (PC) with low (sulfur and V_2O_5 contents) and different five kinds of biomass wastes (rice husk (RH), rice stalk (RS), cotton straw (CS)), by-product wastes (sawdust (SD) and sugar cane bagasse (SCB)) were conducted using a thermogravimetric analyzer (TGA). The kinetics and thermodynamics parameters were estimated using homogeneous model (HM) or the first-order chemical reaction (O1) and shrinking core models (SCM) or Phase boundary controlled reactions (R2 and R3). Biomass wastes improved the blends gasification reactivity. Synergistic effect was observed in the char gasification stage of the blends compared with the pyrolysis stage. Compared to other models the phase boundary controlled reaction (R2) was found to be the best model to predict the experimental data of the co-gasification process. For both reaction stages of single fuels, SD showed the lowest values of activation energy and thermodynamics parameters.

Moreover, in spite of significant on-going research of the thermal conversion technologies such as pyrolysis and gasification for fuel production, there is no information on the reactivity, behaviour, kinetic and thermodynamics of Sudanese date palm frond. Therefore, this study investigates the effect of temperature on reactivity, behaviour, kinetic and thermodynamic parameters of date palm frond at pyrolysis and gasification processes with different temperatures using thermogravimetric analyzer. Homogeneous model (HM) or the first-order chemical reaction (O1) and shrinking core models (SCM) or Phase boundary-controlled reactions (R2 and R3) were used to estimate the kinetics and thermodynamics parameters.

2. MATERIAL AND METHODS

2.1 Materials and sample preparation

In this study, date palm fronds were used. The samples were cut into small pieces and dried naturally. Proximate and ultimate analyses were conducted to obtain the properties of the materials. TGA-2000 (Navas Instruments, Spain) and a Euro-CA 3000 (HEKAtech, Italy) elemental analyser were used following American Society for Testing and Materials (ASTM) D5142. Parr 6300 automatic isoperibol calorimeter was used to estimate the calorific values.

2.2 Thermogravimetric analysis

The thermogravimetric analyser (TGA, NETZSCHSTA 449/F3) was used to investigate the combustion of date palm front under isothermal conditions. A temperature of 800, 900 and 1000 °C at a heating rate of 20 °C min^{-1} was studied. A 5 mg sample was used to avoid the mass transfer effect. The experiments were conducted three times, and the average values were used. The mass loss (TG) and derivative curve (DTG) of the samples were presented as a function of temperature. For the active site Boudouard reactions mechanism (Equation 1, 2, 3 and 4) were considered for char gasification in carbon dioxide domain [17, 18].

ISSN (Online): 2455-3662
EPRA International Journal of Multidisciplinary Research (IJMR) - Peer Reviewed Journal
Volume: 12| Issue: 6| June 2026|| Journal DOI: 10.36713/epra2013 || SJIF Impact Factor 2026: 8.753 || ISI Value: 1.188

$$C + CO_2 \rightarrow 2CO \quad (1)$$

$$C_{fas} + CO_2 \xrightarrow{k_{b1}} C(O) + CO \quad (2)$$

$$C(O) + CO \xrightarrow{k_{b2}} C_{fas} + CO_2 \quad (3)$$

$$C(O) \xrightarrow{k_{b3}} CO \quad (4)$$

Where k_i is the rate of the ith reaction.

2.3 Reactivity measurement

The conversion degree (X) was estimated using Equation (1).

$$X = \frac{w_i - w_t}{w_i - w_f} \quad (5)$$

where w_i is the initial mass sample (mg), w_t is the mass sample at a specific time (min), and w_f is final mass sample at the end of the combustion process. The combustion reactivity was calculated based on the method proposed by Okoroigwe [19] and Edreis et al [20] using Equation (6).

$$R_m = 100 \sum \frac{R_{DTGmax}}{T_{DTGmax}} \quad (6)$$

where R_m is the mean reactivity (% ^{o}C $^{-1}$ min^{-1}), R_{DTGmax} is the maximum weight loss rate (% min^{-1}) and T_{DTGmax} is the corresponding peak temperature (^{o}C). The reactivity indexes $R_{0.1}$, $R_{0.5}$, and $R_{0.9}$ were calculated using Equations (7), (8), and (9) respectively, at different conversion degrees (10%,50%, and 90%) [21, 22].

$$R_{0.1} = \frac{0.1}{t_{0.1}} \quad (7)$$

$$R_{0.5} = \frac{0.5}{t_{0.5}} \quad (8)$$

$$R_{0.9} = \frac{0.9}{t_{0.9}} \quad (9)$$

Where $t_{0.1}$, $t_{0.5}$, and $t_{0.9}$ are the time (min) required to reach the carbon conversion of 10%, 50%, and 90% respectively.

2.4 Kinetic study

The TGA data were used to estimate the kinetic studies of the combustion process. Methods such as the shrinking core models (SCM) or phase boundary controlled reactions (R2 and R3), the homogeneous model (HM), or the first-order chemical reaction (O1) through the Coats–Redfern method, were applied to estimate the kinetic parameters such as activation energy (E) and pre-exponential factor (k_o). The overall reaction rate (dX/dt) of a solid-gas reaction was calculated using Equation (10).

$$\frac{dX}{dt} = k\, f(X) \quad (10)$$

where k is the rate constant (min^{-1}) and f(x) is the reaction mechanism (see Table 1). Assuming that, the partial pressure of the combustion agent remains constant during the process. Based on the temperature, the reaction rate can be described using Arrhenius Equation (11).

$$k = A exp\left(\frac{-E}{RT}\right) \quad (11)$$

where k_o, E and R are the pre-exponential factor (min^{-1}), activation energy (kJ mol^{-1}), and universal gas constant (kJ/mole. K), respectively. The activation energy and pre-exponential factor were related to the reactivity and the material structure, respectively. Reactions with large activation energy require a long reaction time or a higher temperature [20, 23]. The kinetic studies of the DPF combustion were conducted using SCM and HM through Coats–Redfern equation [24], using Equation (12).

$$\ln\left[\frac{g(X)}{T^2}\right] = \ln\left[\frac{k_o R}{\beta E}\left(1 - \frac{2RT}{E}\right)\right] - \frac{E}{RT} \quad (12)$$

where $g(X)$ is the reaction model mechanism used for the calculation of shrinking core models (SCM) and homogeneous model (HM) [25-28]. It is obvious that in Equation (12) the expression $\ln\left[\frac{k_o R}{\beta E}\left(1 - \frac{2RT}{E}\right)\right]$ is basically constant for the value of E in the combustion temperature range [29, 30]. Therefore, the left side of Equation (12) is plotted versus 1/T and a straight line was found. Values of E and k_o were obtained through the slope of the straight line and the intercept of Equation (12), respectively. The HM assumes a homogeneous reaction throughout the particle [28]. The reaction mechanism of the first-order chemical reaction represents the process controlled by the chemical reactions, rather than the effect of intra-particle diffusion, and the reaction happens simultaneously in the whole particle. However, compared to diffusion, the chemical reaction is much faster, therefore, the model R2 and R3 assume the process is controlled by diffusion, rather than the chemical reaction. Moreover, in the SCM the reaction occurs initially at the external surface of the particle and moves gradually to the inside.

ISSN (Online): 2455-3662
EPRA International Journal of Multidisciplinary Research (IJMR) - Peer Reviewed Journal
Volume: 12| Issue: 6| June 2026|| Journal DOI: 10.36713/epra2013 || SJIF Impact Factor 2026: 8.753 || ISI Value: 1.188

Table 1: Expressions of $f(x)$ and $g(x)$ for the kinetic model functions employed for the solid-state reactions [25-28, 31].

Model	Symbol	$f(x)$	$g(x)$
Chemical reaction or homogenous model (HM)			
First-order	O1	$(1-x)$	$-\ln(1-x)$
Phase boundary controlled reactions			
Two dimensions (contracting cylinder)	R_2	$2(1-x)^{\frac{1}{2}}$	$1-(1-x)^{\frac{1}{2}}$
Three dimensions (contracting sphere)	R_3	$3(1-x)^{\frac{2}{3}}$	$1-(1-x)^{\frac{1}{3}}$

2.5 Thermodynamic parameters

Thermodynamic parameters such as enthalpies change (ΔHo, kJ mol-1), Gibbs free energies (ΔGo, kJ mol-1) and entropies change (ΔSo, mol-1.K-1) were calculated using Equations (13), (14) and (15) respectively [32, 33].

$$\Delta H^o = E - RT \quad (13)$$

$$\Delta G^o = E + R.T_m.\ln\left(\frac{K_B.T_m}{h.k_o}\right) \quad (14)$$

$$\Delta S^o = \frac{\Delta H^o - \Delta G^o}{T_m} \quad (15)$$

where, K_B is Boltzmann constant ($1.38X10^{-23}JK^{-1}$), h is Planck constant ($6.626X10^{-34}Js$), T_m is the peak temperature (K) , The change of enthalpies (ΔH^o) demonstrates the energy difference between the activated complex agrees with activation energies and the reagent [33]. However, the values of Gibbs free energies (ΔG^o) showed the growth of overall energy [32]. Whereas, the ΔS^o measures random energy and matter in the DPF combustion [32].

3. RESULTS AND DISCUSSION

3.1 Characterization of date palm frond

The proximate, ultimate, and ash analysis of date palm fronts are shown in Table 2. Higher contents of hydrogen, carbon, oxygen, and volatiles were observed in the date palm front; however, nitrogen and sulfur were lower. The higher heating value was found 15.92 MJ kg^{-1}. Oxygen content was 54.31%; this is considerably higher than that of coal and most of biomasses, hence, a small amount of stoichiometric air could be required for the combustion. The higher value of volatiles (69.84%) indicated its suitability for gasification, pyrolysis, and co-gasification. However, the lower fixed carbon of 12.93% was due to low lignin content in the samples [34]. The ash content was found comparable with that of other biomass [35]. Therefore, DPF found appropriate fuel for continuous thermal processes because of the ash removal and handling problem.

Table 2: Date palm fronds characteristics analysis

Proximate analysis (w%)[a]				Ultimate analysis (w%)[b]					Heating Value		
Ash	VM	FC	M	C	H	O [c]	N	S	HHV	(MJ/kg)[b]	
5.97	69.84	12.93	11.25	39.66	5.47	54.31	0.22	0.34	15.92		

Ash analyses

Mg	Si	P	S	CL	K	Ca	Fe	Mgo	Sio_2	P_2o_5	So_3	Cl_2O	K_2O	CaO	Fe_2O_3
8.61	4.22	4.26	3.94	21.78	42.42	14.55	0.23	12.35	7.33	7.67	7.51	19.31	33.38	12.26	0.19

[a] As received basis.; [b] as Dry ash basis; [c] Calculated by the difference

3.2 Thermal behavior and reactivity analysis at pyrolysis condition

Figure 1 presents the TG and DTG as a function of temperature for the DPF samples investigated. The pyrolysis of DPF was found occurred in one stage at temperature higher than 325 °C. From Table 3, DTG_{max} values were 0.135, 0.155 and 0.165% s-1, at temperature ranges of 164.22─ 366.55 °C, 160.73─ 373.73 °C and 153.76─ 357.93 °C for pyrolysis temperatures of 800, 900 and 1000 °C respectively. Whereas The T_{max} values were 325.91, 329.38 and 329.89 °C for 800, 900 and 1000 °C respectively. This is indicated that DTG_{max} and T_{max} were proportional to pyrolysis temperature. The values of maximum rates of weight loss (DTG)(% s-1) changed from 0.135 to 0.165 at a temperature range of 800─ 1000 °C, found similar to the results reported by Jeguirimand et al. [36]. From Table 2, the reactivities were 0.42 $\times10^{-3}$, 0.47×10^{-3} and 0.51×10^{-3} % s-1 °C-1 for DPF at pyrolysis temperatures of 800, 900 and 1000 °C respectively. A similar results range was obtained by Munir et al. [37] using four different agricultural residues during pyrolysis. Figure 2 shows the variation of the reactivity index against pyrolysis temperature. The reactivity index was found to be proportional to the pyrolysis temperature and increased by 14.96%, 5.07% and 13.22%, respectively, for 800, 900 and 1000 °C.

ISSN (Online): 2455-3662
EPRA International Journal of Multidisciplinary Research (IJMR) - Peer Reviewed Journal
Volume: 12| Issue: 6| June 2026|| Journal DOI: 10.36713/epra2013 || SJIF Impact Factor 2026: 8.753 || ISI Value: 1.188

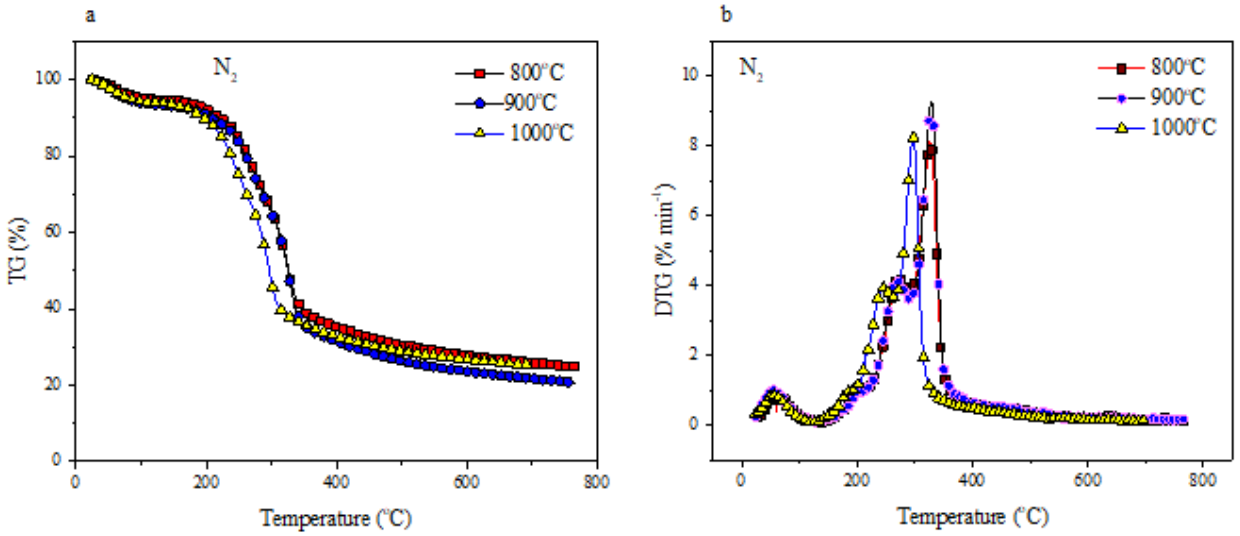

Figure 1: TG and DTG of date palm frond against the temperature at pyrolysis condition.

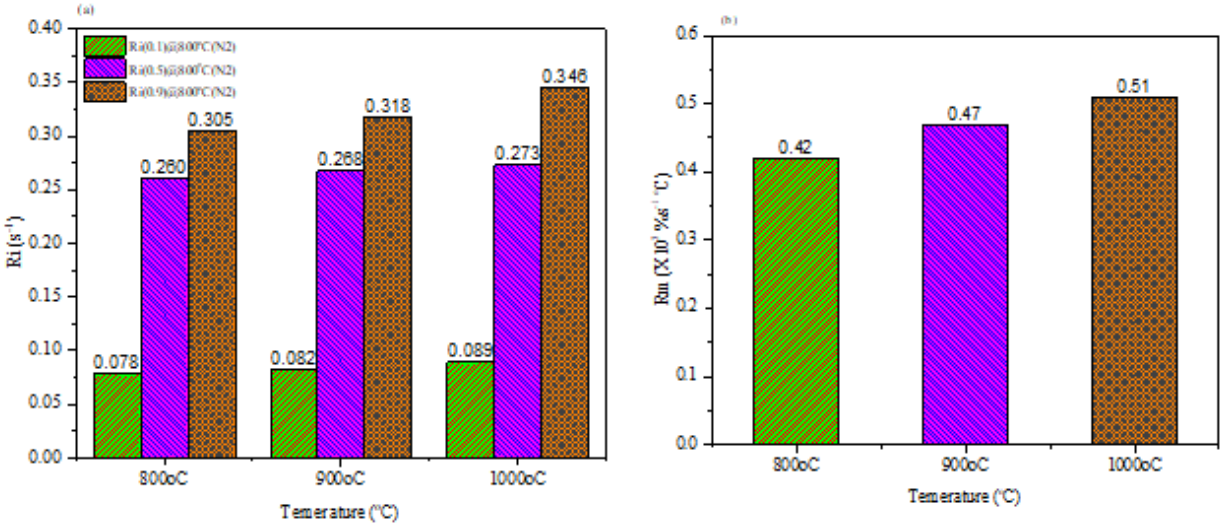

Figure 2: Reactivity (a) and mean reactivity (b) index against the temperature at pyrolysis condition.

Table 3: Pyrolysis characteristics of DPF obtained at different temperatures

Temperature OC	Pyrolysis temp. range (°C)	DTG max % s-1	t max s	T max °C	Rm×10-3 %s-1 oC-1
800	164.22-366.55	0.135	1991	325.91	0. 42
900	160.73-373.73	0.155	2033	329.38	0.47
1000	153.76-357.93	0.165	1941	329.89	0.51

DTG_{max}: maximum pyrolysis rate (% s^{-1}); T_{max}: temperature corresponds to maximum pyrolysis rate (^oC); t_{max}: time corresponds to maximum pyrolysis rate (min); R_m: mean reactivity (% min^{-1} $^oC^{-1}$)

3.3 Thermal behaviour and reactivity analysis at gasification conditions

Figure 3 shows TG and DTG curves for DPF under CO_2 gasification as a function of temperature. The first weight loss found occurred at a temperature < 150 °C. This is attributed to moisture evaporation. Whereas the second weight loss occurred at a temperature range of 150 ─ 380 °C. However, the variation of shapes and the position are seen between 900 to 1000 °C at stage 2. This is due to the reaction of higher volatile matter and lower fixed carbon content in DPF with the gasification agent.

ISSN (Online): 2455-3662
EPRA International Journal of Multidisciplinary Research (IJMR) - Peer Reviewed Journal
Volume: 12| Issue: 6| June 2026|| Journal DOI: 10.36713/epra2013 || SJIF Impact Factor 2026: 8.753 || ISI Value: 1.188

From Table 4, DTG_{max} values were 0. 0.117, 0.155 and 0.135% s-1, while T_{max} values were 326.01, 326.46 and 325.85 ºC, at temperatures of 800, 900 and 1000 ºC respectively. The mean reactivity profiles depicted in Figure 4 were 0.35, 0.52 and 0.48%s-1°C, for temperatures of 800, 900 and 1000 ºC respectively. It concluded that the maximum rate of mass loss was proportional to the reactivity of the sample, while the maximum temperature (Tmax) was inversely proportional to the reactivity. Similar conclusion was reported by Gil et al. [38].

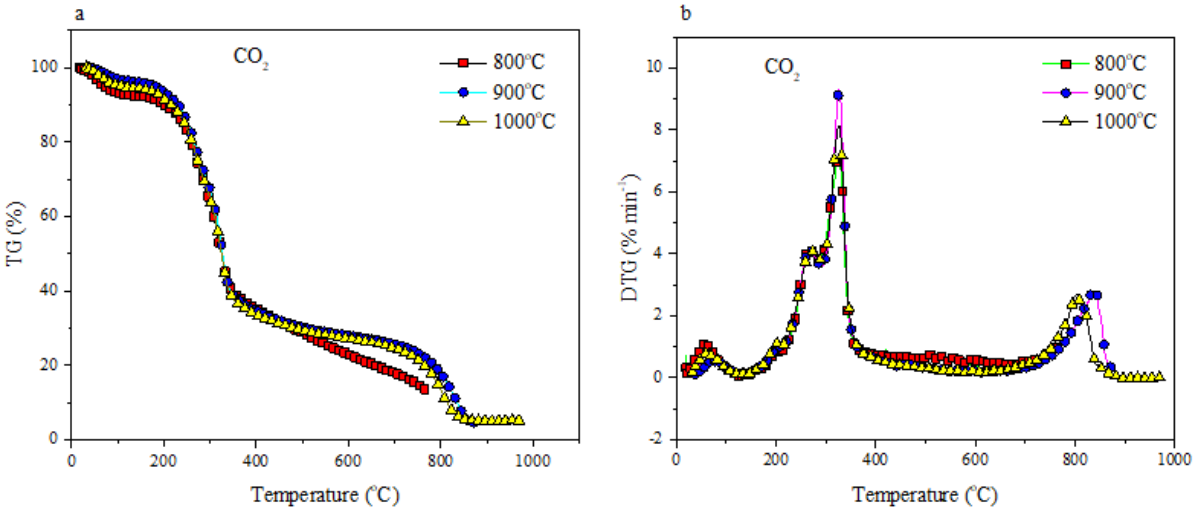

Figure 3: TG and DTG of date palm frond against the temperature at gasification stage.

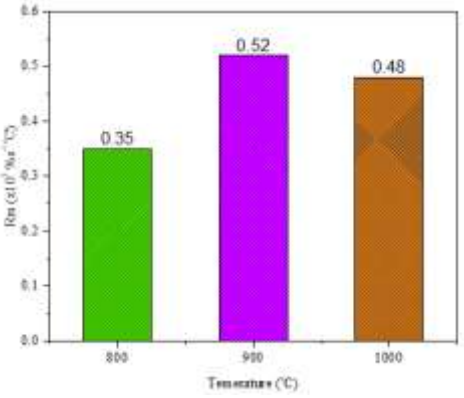

Figure 4: Mean reactivity of DPF as a function of temperature at gasification stage.

Table 4: Characteristics of DPF obtained at different gasification temperatures

Stage (1)					Stage (2)				
Temperature °C	Temperature range °C	DTG max %s-1	t max s	T max °C	Temperature Range °C	DTG max %s-1	t max s	T max °C	Rm×10³ %min-1 °C-1
800	150.88-380.09	0.117	2049	326.01					0.35
900	155.58-373.91	0.155	1987	326.46	697.67-878.24	0.047	5004	839.67	0.52
1000	146.83-381.66	0.135	1964	325.85	682.17-895.57	0.045	4783	804.53	0.48

DTG_{max}: maximum gasifiction rate (% s^{-1}); T_{max}: temperature corresponds to maximum gasification rate (ºC); t_{max}: time corresponds to maximum gasification rate (s^{-1}); R_m: mean reactivity (%s^{-1}°C^{-1}).

3.4 Kinetic and thermodynamic parameters analyses under pyrolysis conditions

The kinetics and thermodynamic parameters investigated are presented in Table 5. Phase boundary controlled reaction (R2) showed the lowest values of activation energy, pre exponential factor and reaction rate, however an opposite trend was observed with first order chemical reaction model (O1). The lowest activation energy value achieved by R2 model was 50.63 kJ/mol

ISSN (Online): 2455-3662
EPRA International Journal of Multidisciplinary Research (IJMR) - Peer Reviewed Journal
Volume: 12| Issue: 6| June 2026|| Journal DOI: 10.36713/epra2013 || SJIF Impact Factor 2026: 8.753 || ISI Value: 1.188

at a pyrolysis temperature of 1000 °C, whereas the highest was 63.15 kJ/mol obtained by O1 model at a pyrolysis temperature of 800 °C. Furthermore, it's found that as the pyrolysis temperature increases, the activation energy, pre-exponential factor and reaction rate decreased. The models of O1, R2, and R3 provided activation energy values in the ranges of 59.37 ─63.15, 50.63 ─ 52.35 and 54.22 ─55.85 kJ mol^{-1} with average values of 61.43, 51.55 and 55.06 kJ mol^{-1}, respectively. Furthermore, the pre-exponential factor achieved by models O1, R2, and R3 ranged from 7.32E+4 ─1.75E+5, 3.82E+03 ─ 5.80E+03 and 6.33E+03 - 9.41E+03 min^{-1}, with average values of 1.20E+05, 4.77E+03 and 7.74E+03 min^{-1} for pyrolysis temperatures of 800, 900 and 1000°C respectively. The correlation coefficient for the models of O1, R2 and R3 was in the range of 0.9887– 0.9980 as presented in Figures 5. This is indicated that the reaction models highly fitted the experimental data. Also, from Table 5, it was found that increasing the pyrolysis temperatures reduced the values of both *E* and *A* for O1, R2, and R3 models. This result agrees with the previous works [39, 40]. In addition, for the thermodynamic parameters from Table 5 it was observed that the change of enthalpies achieved by models O1, R2, and R3 for pyrolysis temperatures of 800, 900 and 1000 °C in the range of 54.38 ─58.17, 45.64 ─ 47.37 and 49.23 ─ 50.87kJ mol^{-1} with average values of 56.32, 46.56 and 50.06 kJ mol^{-1}, respectively. Whereas, models of O1, R2, and R3 provided the values of Gibbs free energies in the ranges of 140.87 – 142.38, 159.35 – 160.39, and 160.44 – 161.49 kJ mol^{-1}, with average values of 141.64, 159.88 and 160.96 kJ mol^{-1} respectively. However, all the models O1, R2, and R3 showed negative values of entropies change (ΔS^o) of -0.142, -0.18873 and -0.18470 kJ mol^{-1}K^{-1}, respectively. Among the models investigated, the model of R2 shows the lowest enthalpy change values, but the lower Gibbs free energy value was obtained by O1 model for all pyrolysis temperatures. It's concluded that the enthalpy change decreases as the pyrolysis temperature increases.

Table 5: Kinetic and thermodynamic parameters at pyrolysis conditions.

Model	Temperature	Kinetic parameters			Thermodynamic parameters		
	°C	*E* (kJ mol^{-1})	*A* (min^{-1})	*K* (min^{-1})	ΔH^o (kJ mol^{-1})	ΔG^o (kJ mol^{-1})	ΔS^o (kJ mol^{-1}.K)
O1	800	63.15	1.75E+5	1.73E+05	58.17	141.69	-0.13945
	900	61.43	1.13E+5	1.12E+05	56.42	142.38	-0.14268
	1000	59.37	7.32E+4	7.23E+04	54.38	140.87	-0.14417
	Average	**61.43**	**1.20E+05**	**1.19E+05**	**56.32**	**141.64**	**-0.1421**
R2	800	52.35	5.80E+03	5.73E+03	47.37	159.35	-0.18697
	900	51.68	4.69E+03	4.64E+03	46.67	160.39	-0.18878
	1000	50.63	3.82E+03	3.77E+03	45.64	159.90	-0.19046
	Average	**51.55**	**4.77E+03**	**4.71E+03**	**46.56**	**159.88**	**-0.18873**
R3	800	55.85	9.41E+03	9.29E+03	50.87	160.44	-0.18295
	900	55.11	7.48E+03	7.39E+03	50.10	161.49	-0.18491
	1000	54.22	6.33E+03	6.26E+03	49.23	160.97	-0.18625
	Average	**55.06**	**7.74E+03**	**7.65E+03**	**50.06**	**160.96**	**-0.18470**

E: Activation Energy, A: pre-exponential factor, *k* (min^{-1}) , ΔH^o: Enthalpies change, ΔG^o: Gibbs free energies and ΔS^o : entropies change.

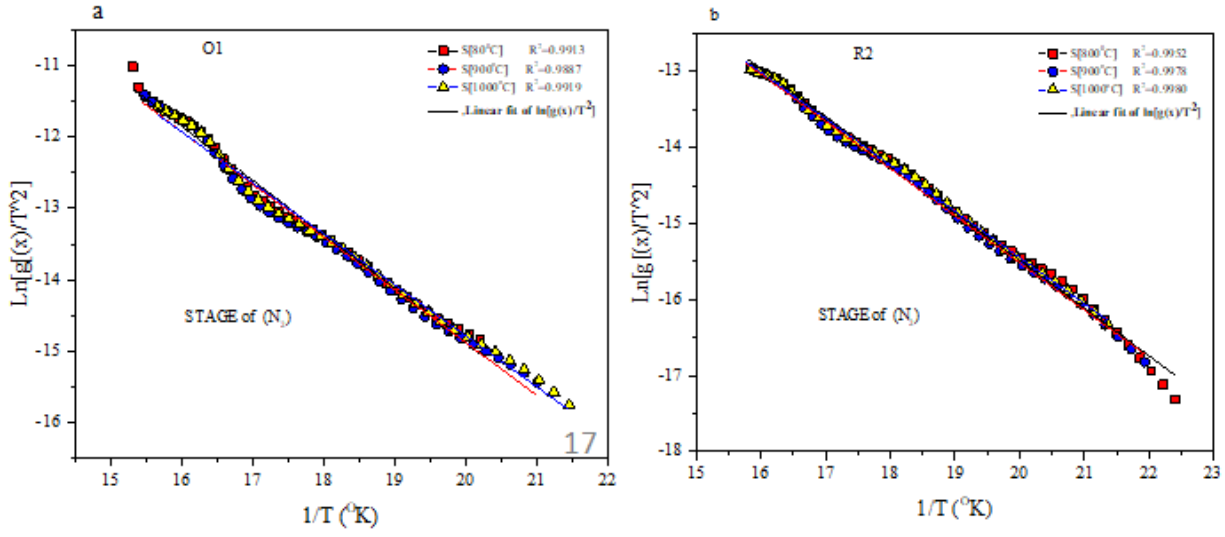

ISSN (Online): 2455-3662
EPRA International Journal of Multidisciplinary Research (IJMR) - Peer Reviewed Journal
Volume: 12| Issue: 6| June 2026|| Journal DOI: 10.36713/epra2013 || SJIF Impact Factor 2026: 8.753 || ISI Value: 1.188

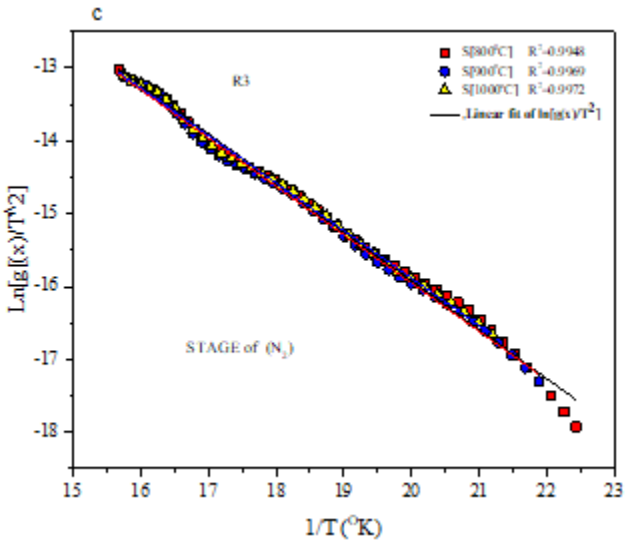

Figure 5: Plots of $ln[g(x)/T^2]$ against $1/T$ with correlation coefficients for DPF at pyrolysis condition (a) Coats–Redfern method; (b) and (c) shrinking core models (SCM).

3.5 Kinetic and thermodynamic parameters analyses under gasification conditions

The correlation coefficient values for the models of O1, R2 and R3 were in ranges of 0.9915– 0.9984, 0.9937 – 0.9907, and 0.9987 – 0.9911, respectively, as presented in Figure 6. All the models showed high correlation coefficients (R2 > 0.991) for the both reaction stages for all of samples. This is indicated that the reaction models highly fitted the experimental data for gasification temperatures of 800, 900 and 1000 °C. The kinetics parameter values of activation energy, pre-exponential factor and reaction rate obtained from the slope of each line in Figure 6 are presented in Table 6. With respect to the kinetic parameters, the pre-exponential factor and activation energy were related to the material structure and reactivity, respectively. Reactions with the high activation energy required high temperature or long reaction time [28]. From Table 6, it was found that for both reaction stages of samples, the lower values of (E, A and k) were achieved by the boundary controlled reactions models (R2 and R3), however the higher values were obtained by the first order chemical reaction model (O1). For stage 1 the lowest value of E, A and K was 50.33 kJ/mol, 3.46E+03 min^{-1} and 3.42E+03 min^{-1} respectively, for gasification temperature 900°C, which was achieved by model R2. However the highest value was 61.79 kJ/mol, 1.32E+05 min^{-1} and 1.30E+05 min^{-1} respectively, for gasification temperature 800 °C, obtained by model O1. For stage 2 the lowest values of E, A and K were 219.69 kJ/mol 5.78E+11 min^{-1} and 5.61E+11 min^{-1} respectively, for temperature 900°C which was provided by model R2. Whereas, the highest value was 293.72 kJ/mol, 1.01E+14 $min^{-1}$and 9.81E+13 min^{-1} respectively, for a temperature 1000 °C, which obtained by model O1. Therefore, it's concluded that the DPF gasification at temperature of 900 °C was more reactive compared to those of 800 and 1000 °C, and the R2 model is most suitable for gasification of DPF.

ISSN (Online): 2455-3662
EPRA International Journal of Multidisciplinary Research (IJMR) - Peer Reviewed Journal
Volume: 12| Issue: 6| June 2026|| Journal DOI: 10.36713/epra2013 || SJIF Impact Factor 2026: 8.753 || ISI Value: 1.188

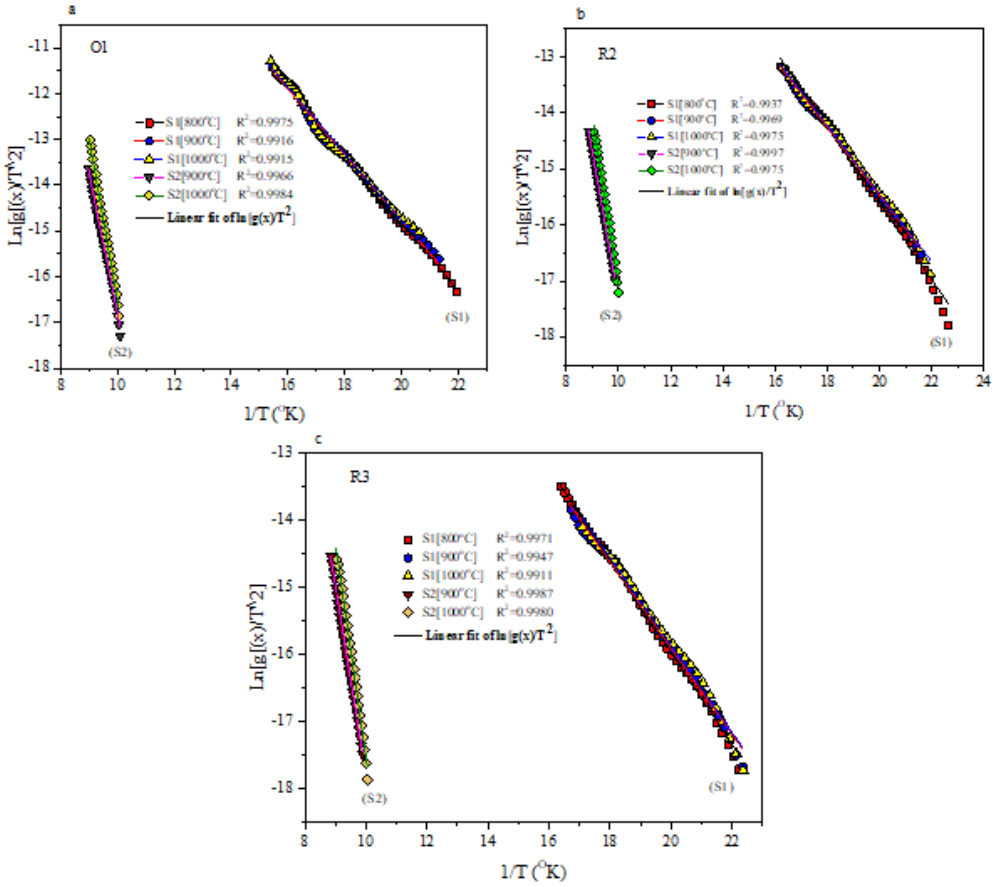

Figure 6: Plots of $ln[g(x)/T^2]$ and ln $[\beta]$ versus $1/T$ with correlation coefficients for DPF at gasification stage (a) Coats–Redfern method; (b) and (c) shrinking core models (SCM).

Table 6: Kinetic parameters of gasification stages.

3.6 Thermodynamic parameters analyses under gasification condition

Temperature (oC)	Models	Stage1 parameters			Stage2 parameters		
		E	A	K	E	A	K
	O1	61.79	1.32E+05	1.30E+05			
800oC	R2	56.65	1.28E+04	1.27E+04			
	R3	57.19	1.59E+04	1.57E+04			
	O1	59.60	7.87E+04	7.77E+04	254.38	5.78E+11	5.61E+11
900oC	R2	50.33	3.46E+03	3.42E+03	219.69	4.35E+09	4.24E+09
	R3	53.48	5.17E+03	5.10E+03	233.09	1.47E+10	1.44E+10
	O1	60.34	9.60E+04	9.48E+04	293.72	1.01E+14	9.81E+13
1000oC	R2	50.46	3.71E+03	3.67E+03	248.72	2.09E+11	2.04E+11
	R3	54.16	6.49E+03	6.41E+03	263.78	8.72E+11	8.46E+11

E: Activation Energy (kJ mol^{-1}), *A*:pre-exponential factor(min^{-1}) *K*: reaction rate (min^{-1})

Thermodynamic parameters of the investigated samples of DPF are shown in Table 7. The changes of enthalpies (ΔH^o) demonstrating the energy difference between the activated complex agreed with activation energies and the reagent [33]. However, the values of Gibbs free energies (ΔG^o) showed the growth of overall energy which would obtainable on the DPF gasification [32]. Whereas the ΔS^o measures random energy and matter in DPF gasification [32]. From the table, It was observed that for both reaction stages, R2 provided the lowest values of the ΔH. Also, it was observed that all the models provided positive values for both ΔH and ΔG and negative values for ΔS. The values of ΔH and ΔG obtained by all models in stage2 were much higher

ISSN (Online): 2455-3662
EPRA International Journal of Multidisciplinary Research (IJMR) - Peer Reviewed Journal
Volume: 12| Issue: 6| June 2026|| Journal DOI: 10.36713/epra2013 || SJIF Impact Factor 2026: 8.753 || ISI Value: 1.188

compared with the values achieved in stage1.While the values of ΔS for the gasification temperatures investigated were almost similar. The gasification temperature of (900 ºC) showed the lowest ΔH and ΔS with values of 45.35 kJmol^{-1} and -0.1912 kJmol^{-1} K^{-1} for stage1and 210.44 kJmol^{-1} and-0.0796 kJmol^{-1}K^{-1} for stage2, respectively, which were obtained by model R2. However, highest values of ΔG was 161.16 kJmol^{-1} for stage1 and 301.18 kJmol^{-1} for stage2, which occurred at gasification temperature of (900 ºC), with the R3 model. Among the models investigated, the model of R2 shows the lowest enthalpy changes, but the lower Gibbs free energy value was obtained by O1 model for stages and all gasification temperatures. Otherwise, the highest Gibbs free energy values were shown by the R3 model.

Table 7: Thermodynamics parameters estimation of gasification stage

	Stage1							
Temperature	**MODEL**	**ΔHº**	**ΔGº**	**ΔSº**		**ΔHº**	**ΔGº**	**ΔSº**
(˚C)								
	O1	56.81	153.26	-0.16100				
800	R2	51.67	158.64	-0.17858				
	R3	52.21	160.26	-0.18037				
	O1	54.62	153.70	-0.16529		245.13	288.53	-0.03900
900	R2	45.35	160.01	-0.19127		210.44	299.07	-0.07965
	R3	48.50	161.16	-0.18794		223.84	301.18	-0.06950
	O1	55.36	153.36	-0.16364		284.76	280.20	0.00423
1000	R2	45.48	159.68	-0.19069		239.76	290.60	-0.04717
	R3	49.18	160.59	-0.18603		254.82	292.88	-0.03532

ΔHº: Enthalpies change, ΔGº: Gibbs free energies and ΔSº : entropies change

4.CONCLUSION

In this study, a Sudanese date palm frond was investigated under pyrolysis and gasification. The samples were characterized and higher heating value, fixed carbon, volatiles and oxygen content were 15.92 MJ kg^{-1}, 12.93%, 69.84% and 54.31% respectively. A common approach was used to model the kinetic parameters of DPF at different temperatures under pyrolysis and gasification conditions. The results indicated that the reactivity, behaviour, kinetics, and thermodynamic parameters were significantly affected by the temperature. Despite the different temperatures, the thermal degradation profiles were similar among the DPF samples. Model R2 was the most effective solid-state mechanism for DPF. Activation energies associated with the devolatilization step in both pyrolysis and two stages of gasification were 52.35, 51.68, and 50.63 kJ mol^{-1} and 59.60, 50.33 and 53.48 kJ mol^{-1} and 254.38, 219.69 and 233.09 for 800, 900 and 1000 ˚C , respectively. DPF at 1000 ºC was the most reactive and showed the lowest E , ΔH^o and ΔS with values of 50.63 kJ mol^{-1}, 45.64 kJ mol^{-1} and -0.190 kJ mol^{-1} K for the pyrolysis process. Furthermore, for gasification at 900 ºC, the DPF provided the lowest E , ΔH^o and $\Delta S°$ with values 50.33 kJ mol^{-1}, 45.35 kJ mol^{-1} and -0.191 kJ mol^{-1} K , respectively for S1 and 219.69 kJ mol^{-1}, 210.44 kJ mol^{-1} and -0.079 kJ mol^{-1} K , respectively for S1 . Finally, all the models are found to be compatible for predicting the experimental data under all temperature values for both processes.

Acknowledgement

The authors would like to acknowledge Prof. Hong Yao for the financial support (Grant No.J17-18-301) and the staff at Key Laboratory of Coal Combustion, Huazhong University of Science and Technology.

REFERENCES

1. *Y. Elmay, M. Jeguirim, G. Trouvé, and R. Said, "Kinetic analysis of thermal decomposition of date palm residues using Coats–Redfern method," Energy Sources, Part A: Recovery, Utilization, and Environmental Effects, vol. 38, pp. 1117-1124, 2016.*
2. *M. Masghouni and M. Hassairi, "Energy applications of olive-oil industry by-products: – I. The exhaust foot cake," Biomass and Bioenergy, vol. 18, pp. 257-262, 2000.*
3. *E. M. Edreis, G. Luo, A. Li, C. Chao, H. Hu, S. Zhang, et al., "CO2 co-gasification of lower sulphur petroleum coke and sugar cane bagasse via TG-FTIR analysis technique," Bioresour Technology, vol. 136, pp. 595-603, May 2013.*
4. *I. Ahmed and A. Gupta, "Kinetics of woodchips char gasification with steam and carbon dioxide," Applied Energy, vol. 88, pp. 1613-1619, 2011.*
5. *C. H. Shen, W. H. Chen, H. W. Hsu, J. Y. Sheu, and T. H. Hsieh, "Co-gasification performance of coal and petroleum coke blends in a pilot-scale pressurized entrained-flow gasifier," International Journal of Energy Research, vol. 36, pp. 499-508, 2012.*
6. *E. M. Edreis, X. Li, G. Luo, S. Sharshir, and H. Yao, "Kinetic analyses and synergistic effects of CO2 co-gasification of low sulphur petroleum coke and biomass wastes," Bioresource technology, vol. 267, pp. 54-62, 2018.*
7. *M. Jeguirim, S. Dorge, G. Trouvé, and R. Said, "Study on the thermal behavior of different date palm residues: characterization and devolatilization kinetics under inert and oxidative atmospheres," Energy, vol. 44, pp. 702-709, 2012.*

ISSN (Online): 2455-3662
EPRA International Journal of Multidisciplinary Research (IJMR) - Peer Reviewed Journal
Volume: 12| Issue: 6| June 2026|| Journal DOI: 10.36713/epra2013 || SJIF Impact Factor 2026: 8.753 || ISI Value: 1.188

8. C. Cardoso, M. Miranda, K. Santos, and C. Ataíde, "Determination of kinetic parameters and analytical pyrolysis of tobacco waste and sorghum bagasse," Journal of Analytical and Applied Pyrolysis, vol. 92, pp. 392-400, 2011.
9. E. C. Okoroigwe, "Combustion analysis and devolatilazation kinetics of gmelina, mango, neem and tropical almond woods under oxidative condition," International Journal of Renewable Energy Research, vol. 5, pp. 1024-1033, 2015.
10. M. Raza, B. Abu-Jdayil, A. H. Al-Marzouqi, and A. Inayat, "Kinetic and thermodynamic analyses of date palm surface fibers pyrolysis using Coats-Redfern method," Renewable Energy, vol. 183, pp. 67-77, 2022.
11. S. A. El-Sayed, T. M. Khass, and M. E. Mostafa, "Thermal degradation behaviour and chemical kinetic characteristics of biomass pyrolysis using TG/DTG/DTA techniques," Biomass conversion and biorefinery, vol. 14, pp. 17779-17803, 2024.
12. A. M. Ali, M. Inayat, A. A. Zahrani, K. Shahzad, M. Shahbaz, S. A. Sulaiman, et al., "Process optimization and economic evaluation of air gasification of Saudi Arabian date palm fronds for H2-rich syngas using response surface methodology," Fuel, vol. 316, p. 123359, 2022.
13. E. Galiwango, A. H. Al-Marzuoqi, A. A. Khaleel, and M. M. Abu-Omar, "Investigation of non-isothermal kinetics and thermodynamic parameters for the pyrolysis of different date palm parts," Energies, vol. 13, p. 6553, 2020.
14. G. Wang, J. Zhang, X. Huang, X. Liang, X. Ning, and R. Li, "Co-gasification of petroleum coke-biomass blended char with steam at temperatures of 1173–1373 K," Applied Thermal Engineering, vol. 137, pp. 678-688, 2018.
15. C. Xu, S. Hu, J. Xiang, L. Zhang, L. Sun, C. Shuai, et al., "Interaction and kinetic analysis for coal and biomass co-gasification by TG–FTIR," Bioresource Technology, vol. 154, pp. 313-321, 2014.
16. E. M. Edreis, X. Li, A. H. Atya, S. W. Sharshir, A. H. Elsheikh, N. M. Mahmoud, et al., "Kinetics, thermodynamics and synergistic effects analyses of petroleum coke and biomass wastes during H2O co-gasification," International Journal of Hydrogen Energy, vol. 45, pp. 24502-24517, 2020.
17. C. Di Blasi, "Combustion and gasification rates of lignocellulosic chars," Progress in energy and combustion science, vol. 35, pp. 121-140, 2009.
18. Z. Huang, J. Zhang, Y. Zhao, H. Zhang, G. Yue, T. Suda, et al., "Kinetic studies of char gasification by steam and CO 2 in the presence of H 2 and CO," Fuel Processing Technology, vol. 91, pp. 843-847, 2010.
19. E. C. Okoroigwe, "Combustion Analysis and Devolatilazation Kinetics of Gmelina, Mango, Neem and Tropical Almond Woods under Oxidative Condition," International Journal of Renewable Energy Research (IJRER), vol. 5, pp. 1024-1033, 2015.
20. E. M. Edreis, X. Li, G. Luo, S. Sharshir, and H. Yao, "Kinetic analyses and synergistic effects of CO 2 co-gasification of low sulphur petroleum coke and biomass wastes," Bioresource technology, vol. 267, pp. 54-62, 2018.
21. Z.-j. Zhou, Q.-j. Hu, X. Liu, G.-s. Yu, and F.-c. Wang, "Effect of iron species and calcium hydroxide on high-sulfur petroleum coke CO2 gasification," Energy & Fuels, vol. 26, pp. 1489-1495, 2012.
22. J. Wei, Y. Gong, Q. Guo, L. Ding, F. Wang, and G. Yu, "Physicochemical evolution during rice straw and coal co-pyrolysis and its effect on co-gasification reactivity," Bioresour Technol, vol. 227, pp. 345-352, Mar 2017.
23. E. Edreis, G. Luo, A. Li, C. Chao, H. Hu, S. Zhang, et al., "CO2 co-gasification of lower sulphur petroleum coke and sugar cane bagasse via TG–FTIR analysis technique," Bioresource technology, vol. 136, pp. 595-603, 2013.
24. A.Coats and J. Redfern, "Kinetic parameters from thermogravimetric data,," Nature, vol. 201, pp. 68-69, 1964.
25. M. Gil, D. Casal, C. Pevida, J. Pis, and F. Rubiera, "Thermal behaviour and kinetics of coal/biomass blends during co-combustion," Bioresource technology, vol. 101, pp. 5601-5608, 2010.
26. S. Y. Yorulmaz and A. T. Atimtay, "Investigation of combustion kinetics of treated and untreated waste wood samples with thermogravimetric analysis," Fuel Processing Technology, vol. 90, pp. 939-946, 2009.
27. A. Aboulkas and A. El Bouadili, "Thermal degradation behaviors of polyethylene and polypropylene. Part I: Pyrolysis kinetics and mechanisms," Energy Conversion and Management, vol. 51, pp. 1363-1369, 2010.
28. E. M. A. Edreis, G. Luo, A. Li, C. Xu, and H. Yao, "Synergistic effects and kinetics thermal behaviour of petroleum coke/biomass blends during H2O co-gasification," Energy Conversion and Management, vol. 79, pp. 355-366, 2014.
29. C. Gong, H. PiWen, X. Bo, H. ZhiQuan, L. ShiMing, Z. LeGuan, et al., "Gasification of biomass micron fuel with oxygen-enriched air: thermogravimetric analysis and gasification in a cyclone furnace," Energy (Oxford), vol. 43, pp. 329-333, 2012.
30. Ö. Çepelioğullar and A. E. Pütün, "Thermal and kinetic behaviors of biomass and plastic wastes in co-pyrolysis," Energy conversion and management, vol. 75, pp. 263-270, 2013.
31. A. Aboulkas, K. El Harfi, and A. El Bouadili, "Thermal degradation behaviors of polyethylene and polypropylene. Part I: Pyrolysis kinetics and mechanisms," Energy Conversion and Management, vol. 51, pp. 1363-1369, Jul 2010.
32. S. R. Naqvi, R. Tariq, Z. Hameed, I. Ali, S. A. Taqvi, M. Naqvi, et al., "Pyrolysis of high-ash sewage sludge: Thermo-kinetic study using TGA and artificial neural networks," Fuel, vol. 233, pp. 529-538, 2018.
33. Y. Xu and B. Chen, "Investigation of thermodynamic parameters in the pyrolysis conversion of biomass and manure to biochars using thermogravimetric analysis," Bioresource Technology, vol. 146, pp. 485-493, 2013/10/01/ 2013.
34. A. Demirbaş, "Relationships between lignin contents and fixed carbon contents of biomass samples," Energy Conversion and Management, vol. 44, pp. 1481-1486, 2003.
35. L. Wang, J. E. Hustad, Ø. Skreiberg, G. Skjevrak, and M. Grønli, "A critical review on additives to reduce ash related operation problems in biomass combustion applications," Energy Procedia, vol. 20, pp. 20-29, 2012.
36. M. Jeguirim and G. Trouvé, "Pyrolysis characteristics and kinetics of Arundo donax using thermogravimetric analysis," Bioresource technology, vol. 100, pp. 4026-4031, 2009.

ISSN (Online): 2455-3662
EPRA International Journal of Multidisciplinary Research (IJMR) - Peer Reviewed Journal
Volume: 12| Issue: 6| June 2026|| Journal DOI: 10.36713/epra2013 || SJIF Impact Factor 2026: 8.753 || ISI Value: 1.188

37. *S. Munir, S. Daood, W. Nimmo, A. Cunliffe, and B. Gibbs, "Thermal analysis and devolatilization kinetics of cotton stalk, sugar cane bagasse and shea meal under nitrogen and air atmospheres," Bioresource technology, vol. 100, pp. 1413-1418, 2009.*
38. *M. a. V. Gil, D. Casal, C. Pevida, J. Pis, and F. Rubiera, "Thermal behaviour and kinetics of coal/biomass blends during co-combustion," Bioresource technology, vol. 101, pp. 5601-5608, 2010.*
39. *I. E. A. a. D. L. C. Ching, " Modified Model for Kinetic Analysis of Petroleum Coke," International Journal of Chemical Engineering, vol. Volume 2019, pp. 1-8, 2019.*
40. *I. M. Hamed Sattar, Shahid Munir, "Thermal and Kinetic Study of Rice Husk, Corn Cobs, Peanut Crust and Khushab Coal under inert (N) and oxidative (dry air) atmospheres," Renewable Energy, 2019.*